Minimax Theory and its Applications
Volume 11 (2026), No. 1, 1-9

Experimental and numerical comparative analysis of piles subjected to lateral loading in granular soil of chilca, peru

Patricio Sanchez[1], Mario Peña[2], Marko Lopez[3]

[1]*Universidad San Ignacio de Loyola, Faculty of Civil Engineering, Lima, Peru*
[2]*Pontificia Universidad Católica del Perú, Faculty of Civil Engineering, Lima, Peru*
[3]*Universidad San Ignacio de Loyola, Faculty of Civil Engineering, Lima, Peru*

Received 10th September, 2025
Accepted 16th December,2025
Published 15th February,2026

Piles are frequently employed in low-strength soils and are often subjected to lateral loads from various phenomena, including wind, waves, earthquakes, and lateral ground pressure. To ensure stability, the lateral strength of the piles must be analysed through theoretical methods or on-site tests, which are essential for accurate design. This research draws parallels between the deflection outcomes of a lateral load test and the responses in the ultimate limit state, p-y, as well as the finite element method. It demonstrates that a range of procedures, with varying degrees of effectiveness, offer a genuine approximation to the behaviour of the pile under lateral loading, thereby facilitating an optimal design. The trial to analyse the experimental behaviour was carried out in Chilca, located in the southern region of Lima, Peru. The full-scale load testing conducted in this location provides a solid basis for understanding the problem. Geotechnical characterization was conducted using standard methods, including SPT field tests and seismic refraction analysis. The properties of the A572 grade 50 tubular steel pile are known to be standardized. The pile that was subjected to lateral load testing was in accordance with the guidelines of the ASTM D3966 standard. A comparison was made between the analytical and numerical calculations and the experimental measurements. This was accomplished by means of displacement plots along the pile. A three-dimensional numerical analysis was performed using the commercial program Abaqus®. This analysis employed an elastoplastic constitutive model with a Mohr-Coulomb failure criterion for the finite element method (FEM). The reaction problem of the subbase (p-y) was solved using GEO5®. The Matlock and Reese approximation was used as the soil modulus. Finally, the Broms and Meyerhof formulations were used for flexible piles.

Keywords: Abaqus, lateral load test, numerical analysis, p-y method.

Introduction

Piles, serving as foundation elements, are frequently utilized in low-strength soils that permit the transfer of compression, tension, and lateral loads to a robust layer of soil. These accumulations are frequently subjected to lateral loads from various external forces, including wind, waves, ship docking, ground pressure, and seismic events (Naveen et al., 2013). Given the high liquefaction potential of these soils, they are also used as foundations for bridges due to the possibility of undermining, as foundations in marine structures, and as a containment measure in the construction of a pile wall. Earthquakes are a latent geological hazard, primarily caused by the subduction of the Nazca Plate under the South American Plate in this region. A historical study of the liquefaction phenomenon in Peru has also been conducted (Alva-Hurtado, 1999). A body of research has emerged on the seismic effects of the Arequipa earthquake in 2001, which led to liquefaction in southern Peru (Audemard, 2001). More recently, the Pisco earthquake in 2007 exhibited comparable consequences (Meneses, 2007). Consequently, it is imperative to acknowledge not only the use of piles in the environment but also their vulnerability to lateral loads.

The study performs a lateral pile loading test, which is then compared with analytical and numerical approaches. A plethora of methodologies have been documented in the extant literature for the analysis of laterally loaded piles. These methodologies can be classified into the following categories: The ultimate limit state (ELU), subgrade reaction approach (p-y), continuous method (not developed in this article), and the finite element

method (FEM) (Moussa & Christou, 2018) are used to determine the stability of the soil. The ELU method conceptualizes the pile as a rigid structure that precipitates imminent failure of the ground. Within this framework, the maximum load that can be applied is determined through equilibrium calculations. The assumption of pile stiffness in its final state is far from accurate, so two variants of the method were used to consider the flexible behaviour (Broms, 1964; Meyerhof et al., 1981; Matlock & Reese, 1962). The maximum ultimate load that could be applied to the pile was subsequently calculated. The subgrade reaction approach method is predicated on the assumption of an elastic behaviour of the soil, where there is a relationship between pressure (p) and settlement (y), at each of the points along the pile. The p-y relationship is delineated by the horizontal reaction modulus. A corresponding relationship was employed for frictional soils (Dessault Systèmes, 2021). Consequently, a 3-D numerical model was developed for a laterally loaded pile using finite element software (Salazar & Tovar, 1983). In the context of geotechnical simulations, the initial soil conditions, including its in-situ stress, are defined in accordance with its depth and specific gravity. The soil is modelled as Mohr- Coulomb elastoplastic, a constitutive model that captures the behaviour of the soil under strain. These methodologies were employed to model a side-loading test that was conducted at PSV's warehouse in Chilca, which is located 43.2 kilometres south of Lima, Peru. A comprehensive characterization of the soil was conducted, encompassing the application of SPT, MASW, and laboratory tests for correlation. This approach was undertaken to ascertain the index and engineering properties of the soil. Therefore, the present study offers the results of a full-scale test and its respective analysis. This provides an opportunity to study the behaviour of piles under lateral loads due to environmental requirements.

1. Theoretical background

The geotechnical investigation and lateral pile testing were carried out at the PSV warehouse in Chilca.

1.1. Soil characterization

As illustrated in Figure 1a, a reference area is delineated on the map of the city of Chilca, while Figure 1b presents a geological map from INGEMMET (Geological, Mining and Metallurgical Institute of Peru). This map indicates that the area corresponds to the alluvial deposit (Qh-al1) of the dejective cones of the Mala River, with thicknesses measured in tens of meters [11]. Furthermore, the seismicity of this region is of particular concern, thus necessitating an in-depth analysis in Chilca (–76° 67′ –12° 44′), where it was ascertained that the maximum acceleration would be approximately 0.43 g. However, for the purpose of a pseudostatic analysis, a maximum of 0.22 g could be considered [12].

On-site analysis was performed using the Standard Penetration Test (SPT) (Skempton, 1986). In the present studies, the evaluation of soil properties is facilitated by empirical correlations, which are contingent upon the number of hits, herein denoted as N. The results obtained from these analyses are presented in Table 1. Notably, the absence of a water table along the borehole was observed. N1(60) corresponds to the corrected number of strokes. The adjustment of the rod length is facilitated by the table of N (Seed, 1976). The correction of the overload is performed with the Seed equation (ASTM, 2020).

The initial value of N is not considered due to its lack of representativeness. The samples were analysed at the Soil Mechanics Laboratory of the PUCP, which facilitated the determination of the following parameters: moisture content (ASTM D4318-17e1, 2020), relative specific weight of solids (ASTM D6913M-17, 2020), granulometry (ASTM D2487-17e1, 2020), and USCS (Terzaghi, 1948). The classification of USCS soils facilitates the unification of the two strata identified: the first, located at a depth of 6 meters, predominantly consists of SM with an SP-SM lens at the 2-meter depth, while the second stratum exhibits greater variability but is predominantly composed of SP-SM with a minor CL-ML lens at a depth of 7 meters. Ohta & Goto (1978) posits that soils with N values, such as the one under consideration, would be classified as dense and very dense.

MASW measurements are the transverse wave velocity (VS) of 200 meters per second (m/s) in the first 5 meters underground and from 5 to 13 meters a VS of 270 m/s. These measurements can be correlated with other

Figure 1: a) Location of the PSV warehouse b) Geological map of INGEMMET (Walsh, 2000).

properties, such as specific gravity and elastic modulus. The results of the SPT permit the correlation of soil properties. Initially, the transverse wave velocity was examined using the correlations of Ohta et al. (1978) (Marto, et al., 2013; JSCE, 1984). The calculation of the friction angle is performed using the equations developed by JSCE (1984) and Peck et al. (1953). The specific gravity is obtained using the equations of Mayne (2001) and Anbazhagan (2020), both of which are dependent on the transverse wave velocity. The elastic properties, such as the modulus of elasticity and Poisson's coefficient, are calculated through correlation with the number of impacts, N. The equations are derived from the works of Bowles (1988), Kuhlawy and Mayne (2021), and for the Poisson coefficient, from Jaky (1944). Horizontal compressibility (nh) is calculated using the correlation of Terzaghi (1955), Décourt (1991), and Leoni (2014). The horizontal reaction modulus of the subsoil (kh) is obtained by the Matlock and Reese equation (1962), and for the passive earth thrust coefficient, the Rankine correlation is used. As demonstrated in Figure 2 and Table 2, the parameters were calculated from geotechnical studies.

Table 1: Measured SPT, soil properties, and USCS classification.

Depth (m)	SUCS	Gs	ω (%)	N	N1 (60)	γ (kN/m³)	N1 (60) By stratum
1 – 1.45	SM	2.69	3.8	83	-	17.05	
2 – 2.45	SP-SM	2.69	7.4	29	33.76	17.05	
3 – 3.45	SM	2.69	11.7	75	81.03	17.05	58.68
4 – 4.45	SM	2.67	14.1	72	73.68	17.05	
5 – 5.45	SM	2.69	17.2	50	46.26	17.05	
6 – 6.45	SP-SM	2.68	14.3	91	85.89	17.56	
7 – 7.45	CL-ML	2.69	32.2	71	61.56	17.56	
8 – 8.45	SM	2.66	13.2	82	65.61	17.56	
9 – 9.45	SP	2.67	15.3	81	60.02	17.56	63.68
10 – 10.45	SP-SM	2.73	19	71	51.41	17.56	
11 – 11.45	SP-SM	2.71	20.5	87	58.59	17.56	
12 – 12.45	SM	2.69	13.8	100	62.71	17.56	

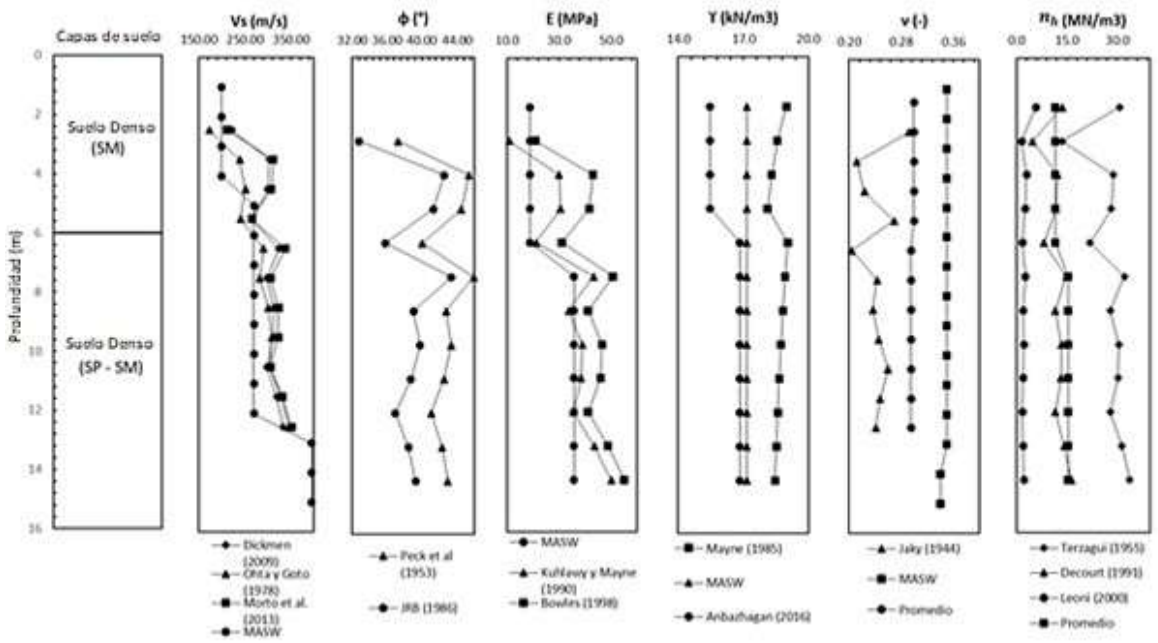

Figure 2: Shear wave velocity, friction angle, modulus of elasticity, Poisson's coefficient, horizontal compressibility constant and specific gravity of the geotechnical investigation.

Table 2: Soil properties. Soil parameters used for modelling.

Depth (m)	ω (%)	γ (kN/m3)	φ (°)	E (MPa)	ν (-)	nh (MN/m3)
0–6	12.60	17.05	38.11	27.71	0.3	11.52
6–13	18.32	17.56	39.37	40.27	0.3	15.42

2. Lateral load test on pile

The primary objective of the lateral load test was to obtain the actual displacement recorded at the top of the pile when subjected to lateral loading. The secondary objective was to determine the load-displacement curve and the displacement of the pile body by means of installed inclinometers. The installation of all piles was executed through the employment of a 24-inch diameter diesel pile hammer (Pileco Inc. D46-32). The pile was driven at a rate of 40 to 60 strokes per minute at the reject level. Two additional piles were identified, positioned at a sufficient distance from the test pile to ensure it did not exert any influence on it. These two piles function as reaction piles. Furthermore, a beam supported by the two reaction piles was placed to simulate a reaction mechanism that prevents deformation and thus obtain the real displacements of the pile. The pile's composition consists of A572 Gr50 steel, which possesses standardized properties. Its specific weight is recorded as 7849.05 kg/m3, while its modulus of elasticity, Poisson ratio, moment of yield, and moment of inertia are measured at 2.105 MPa, 0.3, 1277.72 kN·m, and 0.001061 m4, respectively. To execute the test, the reaction mechanism is composed of two piles that are driven together with a beam resting on them. To ensure the stability of the mechanism, a 100-ton crane is positioned behind the beams to prevent any deformation. As illustrated in Figure 3, the assay is composed of several distinct components, including reaction mechanisms that are installed in the field. After the installation of the reaction mechanism, in conjunction with the pile to be tested, the measuring instruments and the connection mechanism are to be positioned as illustrated in Figure 4. The piston, metal plates, hydraulic jack, and three digital extensometers are to be situated at a height of 0.4 meters above ground level, with an additional two digital extensometers positioned at depths of 1 and 2 meters below ground level, respectively.

The strain gauges positioned at a height of 0.40 meters above the ground facilitate the construction of Figure 5b, which presents the load versus displacement curve at the point of load application. The pile was subjected to a load of 294.3 kN, followed by unloading. As illustrated in Figure 5a, the construction of the strain gauges located 1 and 2 meters below the ground facilitates the measurement of displacements under various applied loads.

3. Numerical Modelling

A three-dimensional model was developed to investigate the behavior of a pile under lateral loading conditions using the Abaqus software (Matlock and Reese, 1962). As illustrated in Figure 6a, the geometry of the numerical model is presented. The pile consists of a tubular section with an external diameter of 24 inches (1/2 inch

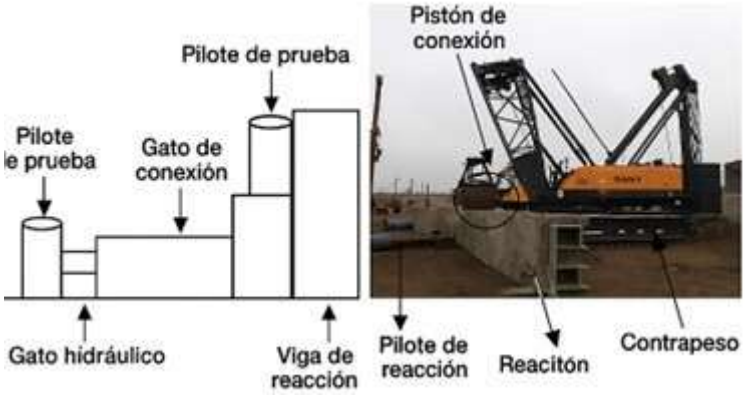

Figure 3: Diagram of the lateral load test and reaction mechanism.

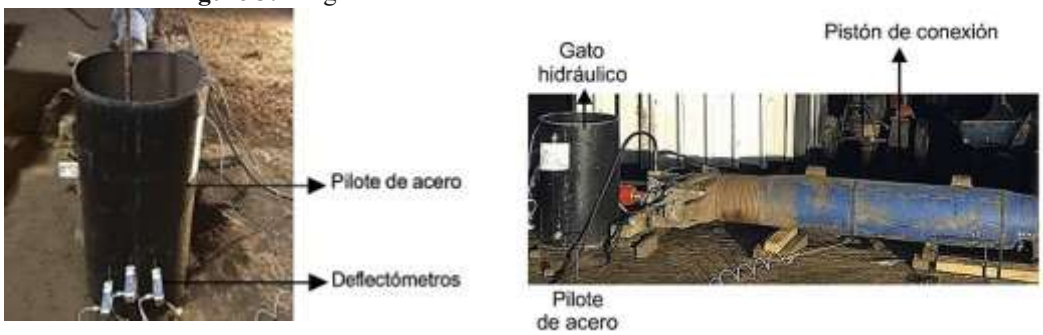

Figure 4: a) Digital strain gauges at the pile head and b) connection mechanism.

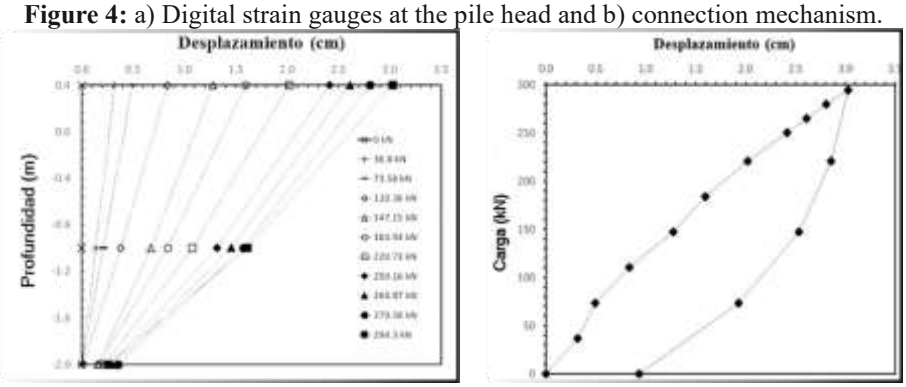

Figure 5. a) Displacements for different loads and b) load versus pile head deflection.

thickness) and a length of 9.2 meters. However, 8.80 meters of this section are buried, and the load is applied at 0.40 meters from the surface level. The geometry of the model is 5 m in diameter and 13 m deep.

The model posits that the interaction between the pile and the ground is governed by a penalty formulation. It is assumed that the pile is in perfect contact with the ground. The interaction between the pile surface and the ground can be described using the normal direction with the “hard” contact type and friction contact, and the tangential direction with the “penalty” contact type and a friction angle value of 20°, following the recommendation of NAVFAC DM 7.2 (NAVFAC, 1984).

The boundary conditions delineate the limits to which there is a physical response to part of the acting loads. This condition manifests at a point where the ground ceases to displace or rotate. The foundation of the sand layer is firmly anchored in the x, y, and z directions, while the displacement of the entire lateral face (x and y) is constrained.

The simulation is executed in two steps. The initial condition is referred to as geostatic equilibrium, wherein in-situ stresses are required to be in equilibrium with the body's strength and the imposed boundary conditions. This option ensures that the initial stress condition is maintained in all elements of all strata, thereby preventing the soil from reaching the creep zone, which, in this case, is defined by the Mohr-Coulomb model. The pile is regarded as a deformable body in accordance with the perfect elastoplastic model, thereby constraining the elasticity to the yield stress of the steel. Subsequently, a lateral load of 294.3 kN is applied, as illustrated in Figure 6b.

Once the above considerations have been made, the program is executed, resulting in a maximum displacement of 3.1 cm, as shown in Figure 7. In addition, the displacements only reach approximately 2.5 m around the pile, so the size of the radius can be considered adequate.

4. Analysis of results

The ultimate limit state functions with a solitary soil layer, thus the properties utilized correspond to the weighted average of the soil along the pile. Broms' ultimate limit state [36] employs equations (1) and (2). The maximum moment is equivalent to the yield moment. Through the application of an iterative resolution, the Zr value is calculated to subsequently ascertain the ultimate horizontal load of the pile.

$$Mmax = my = Hu\left(e + \frac{2}{3}Zr\right) \quad (1)$$

$$Hu = 1.5\gamma BK_{pZr2} \quad (2)$$

Meyerhof's ultimate limit state [8] formulates equations (3), (4) and (5) that relate the stiffness of the soil and the pile to quantify the effective length of the pile and then calculate the applicable ultimate load.

$$Krs = \frac{EpIp}{E\,L4_n} \quad (3)$$

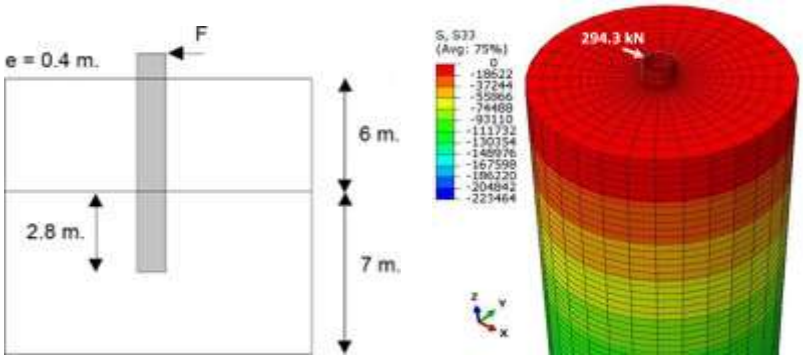

Figure 6: a) Model schematic and b) load allocation and geostatic balancing.

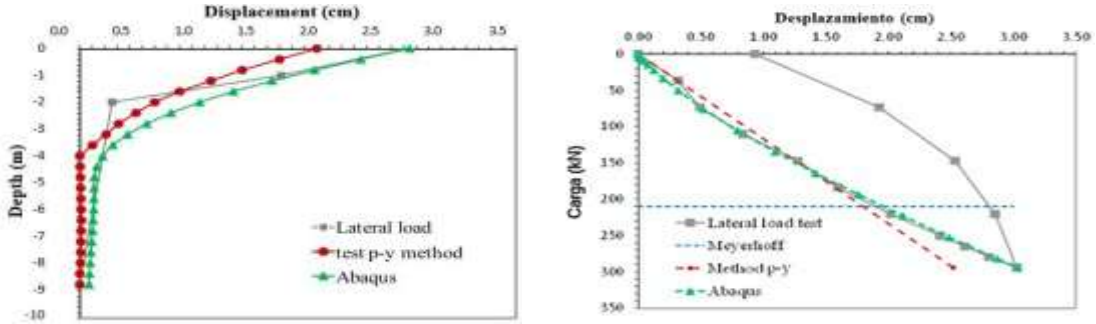

Figure 8: a) Displacement along the length of the pile and b) load vs. displacement.

(4)

$$Le = L1.65K_{rs0.12}$$
$$Hu = 0.12\gamma BL_{e2Kp} \quad (5)$$

The ultimate limit state allowed the ultimate horizontal load to be calculated; in the cases of Broms and Meyerhof, it was 550 kN and 210 kN, respectively. The differential equation (6) developed to solve this method allowed the calculation of the displacement obtained, which was 2.5 cm, and the maximum moment, of approximately 499 kN·m, at 2.3 m below ground level.

$$EpIp\frac{D4y}{dx4} + Px\frac{D2y}{dx2} + khDy = 0 \quad (6)$$

The results obtained with the different methods yield response values within an adequate magnitude range. Figure 8 shows a comparison of the displacements as a function of load and the displacements along the pile. The results of these analyses can help reduce costs and avoid oversizing by reducing uncertainty in the face of potential pile failures.

Conclusions

The stress-strain behaviour of piles is a critical factor to consider in the design of piles subjected to lateral loads, particularly in regions with an elevated risk of seismic activity. The findings of these analyses have the potential to contribute to cost reduction and the prevention of oversizing by decreasing uncertainty in the event of a potential pile failure.

The ultimate limit methods are characterized by a high degree of imprecision. The Broms method yields an ultimate load that significantly exceeds the loads calculated by the other methods. The Meyerhof method utilizes the ratio of the modulus of elasticity between the soil and the steel, thereby yielding a more conservative value. In cases where behaviour is predominantly flexible, Meyerhof's method is particularly suitable.

The p-y method yielded a similar magnitude of lateral displacement; however, the moment found was well below the yield strength. This is not compatible with the results of the test, since the pile presented a permanent deformation, which caused it to enter the plastic regime. At loads ranging up to approximately 160 kN, the results obtained from the model and the test exhibited a high degree of similarity. This discrepancy could be attributed to the fact that, when the applied load is less than 160 kN, the elastic assumptions inherent in the p-y method are more precise.

The numerical method demonstrates the greatest similarity in the displacement response. This is attributable to an optimal selection of the diameter of the designated land, the characterization that was validated through two distinct tests, and an adequate simulation of the initial stresses of the soil.

The distinction among these three methodologies lies in the assumptions that were made during their development. In the case of the p-y method, the elasticity regime can be simulated with a high degree of accuracy up to a load of 180 kN. However, after this load is reached, the plastic displacements increase, and the curves begin to separate. In contrast, the numerical model can better resemble the behaviour observed in the test.

Acknowledgements

The authors gratefully acknowledge all the experts for their time, devotion and precious contributions to the study. Furthermore, the authors are grateful to the reviewers for the precious suggestions provided to improve the overall quality of the investigation.

Funding

The research was conducted independently by the researchers, and no funding was received.

Author contributions

PS, MP and ML designed the study. PS, MP and ML collected data. PS, MP and ML curated and analyzed the dataset. PS and MP wrote the first version of the manuscript. ML supervised the project. PS, MP and ML arranged funding. All authors read, reviewed and approved the final version of the manuscript.

Disclosure statement

The authors declare that the research was conducted in the absence of any commercial or financial relationships that could be construed as a potential conflict of interest.

References

1. Alva-Hurtado, J. E. (1999). Soil liquefaction in Peru. En *Earthquake Geotechnical Engineering: Proceedings of the 2nd International Conference on Earthquake Geotechnical Engineering* (Vol. 3, pp. 1035–1042). A. A. Balkema. *(Nota: Se asumió que A. A. Balkema es el editor para las actas).*
2. Anbazhagan, P., Uday, A., & Moustafa, S. S. R. (2018). Correlation of densities with shear wave velocities and SPT N values. *Journal of Geophysics and Engineering, 13*(3), 320. https://doi.org/10.1088/17422132/13/3/320
3. ASTM International. (2020). *ASTM D1586/D1586M-18. Standard Test Method for Standard Penetration Test (SPT) and Split-Barrel Sampling of Soils*. West Conshohocken, PA: Autor.
4. ASTM International. (2020). *ASTM D2216-19. Standard Test Methods for Laboratory Determination of Water (Moisture) Content of Soil and Rock by Mass*. West Conshohocken, PA: Autor.
5. ASTM International. (2020). *ASTM D2487-17e1. Standard Practice for Classification of Soils for Engineering Purposes*. West Conshohocken, PA: Autor.
6. ASTM International. (2020). *ASTM D4318-17e1. Standard Test Method for Specific Gravity of Soil Solids by Gas Pycnometer*. West Conshohocken, PA: Autor.
7. ASTM International. (2020). *ASTM D6913M-17. Standard Test Methods for Particle-Size Distribution (Gradation) of Soils Using Sieve Analysis*. West Conshohocken, PA: Autor.
8. Audemard M., F. A., Gómez, J. C., Tavera, H. J., & Orihuela G., N. (2005). Soil liquefaction during the Arequipa Mw 8.4, June 23, 2001 earthquake, southern coastal Peru. *Engineering Geology, 78*(3–4), 237–255. https://doi.org/10.1016/j.enggeo.2004.12.007
9. Bowles, J. E. (1988). Elastic foundation settlements on sand deposits. *Journal of Geotechnical Engineering, 113*(8), 846–860. *(Nota: El número 21705 fue omitido ya que parece ser un identificador de artículo o número de serie, no el número de la edición o volumen).*
10. Broms, B. B. (1964). Lateral resistance of piles in cohesionless soils. *Journal of the Soil Mechanics and Foundations Division, 90*(3), 123–156.
11. Broms, B. B. (1964). Lateral resistance of piles in cohesionless soils. *Journal of the Soil Mechanics and Foundations Division, 90*(3), 123–156. *(Nota: Referencia duplicada de la original #7).*
12. Décourt, L. (1991). Load-deflection prediction for laterally loaded piles based on N-SPT values. En *Proceedings of the 4th International Conference on Piling and Deep Foundations* (pp. 549–556). International Society for Soil Mechanics and Geotechnical Engineering.
13. Dessault Systèmes. (2021). *Abaqus Documentation*.
14. Dikmen, Ü. (2009). Statistical correlations of shear wave velocity and penetration resistance for soils. *Journal of Geophysics and Engineering, 6*(1), 61–72. https://doi.org/10.1088/1742-2132/6/1/007
15. Jáky, J. (1944). The coefficient of earth pressure at rest. *Journal of the Society of Hungarian Architects and Engineers*, 355–358.
16. JSCE. (1984). *Earthquake Resistant Design for Civil Engineering Structures in Japan*.
17. Kulhawy, F. H., & Mayne, P. W. (1990). *Manual on estimating soil properties for foundation design* (No. EPRI-EL-6800). Electric Power Research Inst. *(Nota: Se asumió 1990 como año, ya que es el año de la publicación EPRI-EL-6800. La editorial es el Electric Power Research Inst.).*
18. Leoni, A. J. (2014). *Apunte de Coeficiente de Balasto*. Academia.edu. Recuperado de https://unlp.academia.edu/ProfIngAugustoJos%C3%A9Leoni *(Nota: Se formateó como un trabajo recuperado de un sitio web, y se usa el nombre del sitio web como fuente en lugar de la editorial, ya que es una publicación auto-archivada).*
19. Marto, A., Tan, C. S., & Leong, T. K. (2013). Universal correlation of shear wave velocity and standard penetration resistance. *Electronic Journal of Geotechnical Engineering, 18 M*, 2727–2738.

20. Matlock, H., & Reese, L. C. (1962). Generalized solutions for laterally loaded piles. *Transactions of the American Society of Civil Engineers, 127*(1), 1220–1248.
21. Matlock, H., & Reese, L. C. (1962). Generalized solutions for laterally loaded piles. *Transactions of the American Society of Civil Engineers, 127*(1), 1220–1248. *(Nota: Referencia duplicada de la original #9).*
22. Mayne, P. W. (2001). Stress-strain-strength-flow parameters from enhanced in-situ tests. En *Int. Conf. In-Situ Meas. Soil Prop. Case Hist.* (pp. 27–48). *(Nota: Se asume que es una contribución a actas de conferencia).*
23. Meneses, J. F. (2007). Case Histories of Widespread Liquefaction and Lateral Spread Induced By the 2007 Pisco, Peru Earthquake. *(No. 4, pp. 1–6). (Nota: Falta el nombre de la revista/publicación).*
24. Meyerhof, A. J., Mathur, S. K., & Valsangkar, A. J. (1981). Lateral resistance and deflection of rigid walls and piles in layered soils. *Canadian Geotechnical Journal, 18*(2), 159–170.
25. Moussa, A., & Christou, P. (2018). *The Evolution of Analysis Methods for Laterally Loaded Piles Through Time* (No. August 2019). *(Nota: Se asume que es un informe técnico o trabajo no publicado, y la fecha del informe es 2018).*
26. Naveen, B. P., Sitharam, T. G., & Vishruth, S. (2013). Numerical Simulations of Laterally Loaded Piles. *doi: 10.3850/978-981-07-3560-9_09-0907 (Nota: Se asume que es una publicación con DOI, pero falta el nombre de la fuente o actas de conferencia).*
27. Ohta, Y., & Goto, N. (1978). Empirical shear wave velocity equations in terms of characteristic soil indexes. *Earthquake Engineering & Structural Dynamics, 6*(2), 167–187. https://doi.org/10.1002/eqe.4290060205
28. Peck, R. B., Hanson, W. E., & Thornburn, T. H. (1953). *Foundation Engineering*. John Wiley and Sons.
29. Salazar Díaz, C., & Landa Tovar, H. (1983). *Geología de los cuadrángulos de Mala, Lunahuaná, Tupe, Conayca, Chincha, Tantará y Castrovirreyna 26-j, 26-k, 26-l, 26-m, 27-k, 27-l, 27-m*. *(Nota: Se asume que es una publicación no periódica o informe).*
30. Seed, H. B. (1976). *Evaluation of Soil Liquefaction Effects on Level Ground During Earthquakes* (ASCE Natl. Conv., Vol. ASCE Speci, pp. 1–105). *(Nota: Se asume que es un documento de convención o informe).*
31. Skempton, A. W. (1986). Standard penetration test procedures and the effects in sands of overburden pressure, relative density, particle size, ageing and overconsolidation. *(No. 3, pp. 425–447). (Nota: Falta el nombre de la revista/publicación).*
32. Terzaghi, K. (1955). Evaluation of coefficients of subgrade reaction. *Géotechnique, 5*(4), 297–326.
33. Terzaghi, K., Peck, R., & Mesri, G. (1996). *Soil Mechanics in Engineering Practice* (3.ª ed.). John Wiley and Sons. *(Nota: El año original es 1948; se ha actualizado a una edición posterior común, o se puede usar (1948) si se hace referencia a esa primera edición. Se usó el formato para la 3.ª edición común, publicada póstumamente o con revisiones).*
34. U.S. Department of the Navy. (1984). *Foundation and Earth Structures* (NAVFAC DM. 7). *(Nota: Se asume que NAVFAC DM. 7 es la serie o número de publicación).*
35. Walsh, P. (2000). *Estudio de Impacto Ambiental y Social de los Sistemas de Transporte de Gas Natural y Transporte de los Líquidos de Gas* (Vol. II, pp. 1–19). *(Nota: Se asume que es un informe/libro sin editorial o lugar de publicación especificado).*